ORIGINAL ARTICLE

A. V. Porubov◉ · A. M. Krivtsov

Dispersive propagation of localized waves in a mass-in-mass metamaterial lattice

Abstract Linear localized waves evolution in a discrete mass-in-mass lattice is studied. The presence of the attached mass in the model contributes to dispersion giving rise to appearance of both the acoustic and optic wave modes. Important features of the waves are described using the dispersion relation, which is obtained in a continuum limit of the original discrete equations using a harmonic wave solutions. We study numerically the localized initial perturbations evolution and compare the features of the numerical solutions with those obtained for the analytical harmonic wave ons. We have found differences in the wave dynamics depending on the parameters of the initial conditions. One scenario describes almost permanent shape and velocity counterpart localized waves propagation with oscillating standing wave around the position of the initial pulse. Another wave evolution accounts for a decrease in the moving wave amplitude with the developing oscillating tail behind the localized wave. Contrary to the periodic analytical solution, no evidence of a band gap is found in the simulations of localized waves.

Keywords Metamaterial lattice · Continuum limit · Localized wave · Group velocity · Dispersion relation

1 Introduction

The study of discrete crystalline lattices with a complex structure draw considerable attention, in particular, in relation with the description of the materials with microstructure. While all nodes in simple lattices are equivalent, complex lattices are characterized by the presence of different nodes, or, alternatively, a complex lattice can be thought as a combination of several simple sub-lattices [1–3]. Complex structure of the lattices brings additional degrees of freedom, allowing effective modeling of mechanical [2–8] and heat transfer [9–12] processes in solids. Among the discrete complex models considerable attention is paid to the acoustic metamaterials [4,13–17]. One of the simplest but instructive metamaterial models is the mas-in-mass lattice model, see, e.g., [13,14]. It allows to describe the band gap in the dispersion relation, negative effective mass and other features related to a metamaterial, see, e.g., [18,19]

Propagation or non-propagation of acoustic waves in an acoustic metamaterial is its important feature from the point of view of its practical use. At the same time, the linear wave analysis resulting in obtaining the dispersion relations is based on an analysis of a monochromatic harmonic wave solution. What happens when the localized waves are considered? Is it still possible to use these analytical estimations? Success of

---

A. V. Porubov (✉) · A. M. Krivtsov
Institute for Problems in Mechanical Engineering, Bolshoy 61, V.O., St. Petersburg, Russia
E-mail: alexey.porubov@gmail.com

A. M. Krivtsov
Peter the Great St. Petersburg Polytechnic University, Polytechnicheskaya St., 29, St. Petersburg, Russia

kinetic [20–25] and energy dynamics [26,27]-based approaches in description of heat and energy transfer in solids confirms efficiency of the monochromatic consideration for the localized harmonic waves. However, this situation is less understood for complex lattices, and the current paper is devoted to analysis of the related questions on the base of relatively simple, but fairly fruitful mass-in-mass model.

Thus, in this paper we study numerically generation of localized waves in a linear mass-in-mass lattice.

In Sec. 2 we consider a pair of coupled linear partial differential equations, describing dynamics of the main and attached masses of the lattice, where the continuum limit of the original discrete model is concerned. The predictions of the conventional analysis based on the harmonic waves consideration will be studied numerically in Sec. 3 for the localized initial perturbations. The conclusions summarize the paper.

2 Basics of the model

Consider a chain where interaction between the masses, m, is modeled by linearly elastic springs. Also the additional masses, m_1, are attached by the springs to each mass m in the main chain, and this interaction is also linear and elastic [14]. Masses m_1 do not interact directly between themselves. The displacement of the mass m with the number n is denoted by u_n, while that of m_1 is denoted by v_n. Then the equations of motion are [14]:

$$\ddot{u}_n = \beta_0(u_{n-1} - 2u_n + u_{n+1}) + \eta\beta_1(v_n - u_n), \tag{1}$$
$$\ddot{v}_n = -\beta_1(v_n - u_n). \tag{2}$$

Here $\eta = m_1/m$, while the linear stiffness of the spring of the main chain is $\beta_0 m$, and the stiffness of the attached spring is $\beta_1 m_1$.

We proceed with a continuum limit of Eqs. (1), (2). Following the standard procedure, we introduce the continuum functions $u(x, t)$, $v(x, t)$ for description of the displacements of the masses m, m_1. Variable x is the spatial coordinate, such as $x = nh$ in the lattice nodes, where h is the lattice step. The continuum displacements of the neighboring masses are sought using the long-wave approximation [1], based on the Taylor series, where the lattice step, h, is considered as an increment of the spatial variable, x. Retaining only the first nonzero term in the expansion, we obtain

$$u_{tt} = a^2 u_{xx} + \eta\beta_1(v - u), \tag{3}$$
$$v_{tt} = -\beta_1(v - u), \tag{4}$$

where $a = \sqrt{\beta_0}\, h$ is the long-wave velocity for the main lattice. In the absence of coupling, $\eta = 0$, equation for u is the conventional linear wave equation, whose d'Alembert solution describes wave propagation with the phase velocity equal to a.

In the general case, the conventional harmonic traveling wave solution is sought as

$$u = A \exp\Big(\iota\, p\, (x - V t - x_0)\Big), \qquad v = B \exp\Big(\iota\, p\, (x - V t - x_0)\Big), \tag{5}$$

where x_0 accounts for an initial position of the wave, A and B are the wave amplitudes, p is the wave number, V is the wave velocity, ι is the imaginary unit. Substitution of Eq. (5) into Eqs. (3), (4) results in the relationship between A and B,

$$A = \frac{B(\beta_1 - p^2 V^2)}{\beta_1}, \tag{6}$$

and the dispersion relation whose solutions are $V = V_a$, $V = V_o$, where

$$V_a^2 = \frac{\beta_1(1 + \eta) + a^2 p^2 - \sqrt{(\beta_1(1 + \eta) + a^2 p^2)^2 - 4\beta_1 p^2 a^2}}{2p^2}, \tag{7}$$

$$V_o^2 = \frac{\beta_1(1 + \eta) + a^2 p^2 + \sqrt{(\beta_1(1 + \eta) + a^2 p^2)^2 - 4\beta_1 p^2 a^2}}{2p^2}. \tag{8}$$

The limiting values for the phase velocities are collected in Table 1. For $p \to 0$ velocity V_a tends to the long-wave limiting value $a_1 = a/\sqrt{1 + \eta}$, while V_o tends to infinity as $\sqrt{\beta_1(1 + \eta)}/p$. The V_a vanishes at $p \to \infty$ as $\sqrt{\beta_1}/p$, while V_o tends to the finite value equal to a. One has to note that a is the velocity of the

Table 1 Limiting values for the main velocities, where $a_1 = a/\sqrt{1+\eta} \leq a$

p	V_a, V_{ga}	V_o	V_{go}
0	a_1	∞	0
∞	0	a	a

Here V_a and V_o are the phase velocities, V_{ga} and V_{go} are the group velocities; indexes a and o denote the velocities for acoustic and the optic waves, respectively

wave of the linear wave equation arising from Eq.(3) at $\eta = 0$. It is informative to depict the relative values of the velocities. Then the variation of the relative velocities in p reveals a band gap lying inside the interval $(1/\sqrt{1+\eta},\ 1)$, as shown by dashed lines in Fig. 1. Analogous results have been obtained for the investigated Maxwell model theoretically in [28] and experimentally in [29]. Both the acoustic and optic velocities decrease in p; however, the acoustical branch decreases up to zero but the optic wave velocity tends to a.

The group velocity, V_g, is defined as

$$V_g = \frac{\partial(V\,p)}{\partial p}.$$

For $V = V_a$ we obtain

$$V_{ga} = \frac{a^2}{2V_a}\left(1 - \frac{a^2 p^2 - \beta_1(1-\eta)}{\sqrt{\left(a^2 p^2 + \beta_1(1+\eta)\right)^2 - 4a^2\beta_1 p^2}}\right),$$

while for $V = V_o$ we obtain

$$V_{go} = \frac{a^2}{2V_o}\left(1 + \frac{a^2 p^2 - \beta_1(1-\eta)}{\sqrt{\left(a^2 p^2 + \beta_1(1+\eta)\right)^2 - 4a^2\beta_1 p^2}}\right).$$

The limiting values for the group velocities together with the phase velocities are given in Table 1. For $p \to 0$ velocity V_{ga} tends to a_1, while V_{go} tends to zero. The V_{ga} vanishes at $p \to \infty$, while V_{go} tends to the finite value equal to a. Typical group velocity curves are shown in Fig. 2. There is no band gap contrary to the phase velocities shown in Fig. 1.

The predictions about the band gap and the dependence of the phase velocity on p are done on the basis of the harmonic solution (5). What happens with the evolution of a localized perturbation?
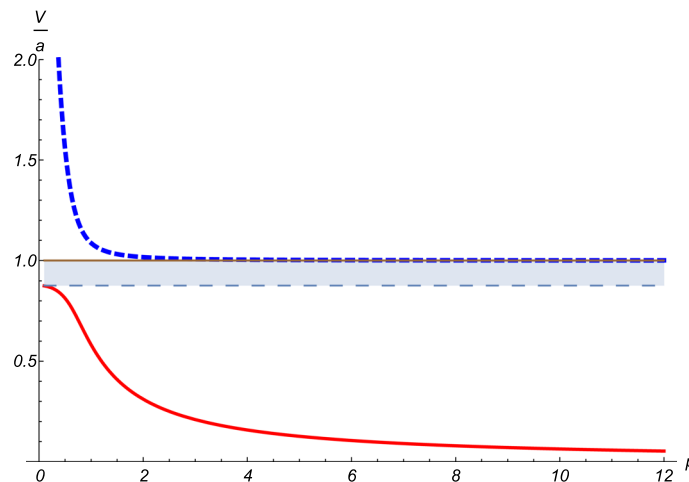
Fig. 1 Variation of the relative phase velocities with the wave number, p, for $\eta = 0.3$. The red solid curve stands for the decay of the relative acoustic velocity, V_a/a as $p \to \infty$; the blue short-dashed curve is the optic velocity, V_o/a; the horizontal long-dashed lines are the asymptotes corresponding to the limiting value of V_o/a at $p \to \infty$ and V_a/a at $p = 0$ (color figure online)
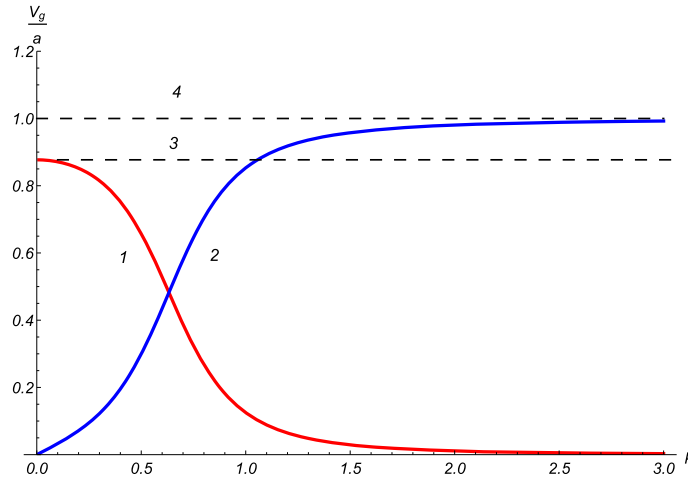
Fig. 2 Variation of the relative group velocities with the wave number, p, for $\eta = 0.3$. 1. The decay of the relative acoustic velocity, V_a/a as $p \to \infty$ shown by red solid line. 2. The blue solid curve is the relative optic velocity, V_{go}/a, (2). 3. The limiting value of V_{ga}/a at $p = 0$ shown by dashed line. 4. The limiting value of V_{go}/a at $p \to \infty$, (color figure online)

Let us consider case $\eta = 0$, then Eq. (3) is reduced to the linear wave equation

$$u_{tt} = a^2 u_{xx}, \tag{9}$$

where the conventional d'Alembert solution holds. When the initial disturbance is a localized pulse, $Q(x)$, and the initial velocity of the disturbance is zero, the solution of Eq. (9) is

$$u = \frac{1}{2} Q(x - at) + \frac{1}{2} Q(x + at).$$

The solution accounts for localized propagation of equal pulses with the same wave velocity a. When the initial conditions are

$$u(x, 0) = Q(x), \qquad u_t(x, 0) = -W Q_x(x), \tag{10}$$

where W is a positive constant providing a nonzero velocity of the initial perturbation. Then the solution of Eqs. (9), (10) is

$$u = \frac{a + W}{2a} Q(x - at) + \frac{a - W}{2a} Q(x + at). \tag{11}$$

Then unidirectional propagation happens only at $W = a$. The positive amplitude waves propagate in both directions when $W < a$, while a negative amplitude wave moves to the left at $W > a$. Non zero η adds dispersion in the behavior of the waves, and d'Alembert solution does not exist anymore, so the further analysis will be performed numerically.

3 Localized waves evolution

The Wolfram Mathematica command $NDSolve$ is used to numerically solve Eqs. (3), (4) and to describe the evolution of the localized waves u and v. The Wolfram Language function NDSolve is a general numerical differential equation solver. The calculations are performed in the spatial interval $(0, x_N)$ and the temporal interval $(0, t_N)$. The periodic boundary conditions are used for the functions u and v. The initial conditions will be specified later. The chosen value of x_N is shown in the figures, the value of t_N takes on different values, which are marked on the figure captions. We choose the initial position of the localized disturbance in the vicinity of the central point $x_0 = x_N/2$.

Consider first an evolution of an initially localized perturbation in the form of the initially motionless Gaussian distribution,

$$u(x, 0) = F \exp\left(-k(x - x_0)^2\right), \qquad u_t(x, 0) = 0, \tag{12}$$

$$v(x, 0) = G \exp\left(-k(x - x_0)^2\right), \qquad v_t(x, 0) = 0, \tag{13}$$

where F, G, x_0, k are constants. The constant values for the calculations are chosen as $k = 0.005$, $F = 0.6$, $G = 1$. The values of the coefficients of the equations (3), (4) are assumed to be $a = 0.5$, $\beta_1 = 0.1$. The mentioned values were chosen after numerous experiments in a wide range of parameters, aiming to find the most representative values. The coupling coefficient η varies in the simulations being presented below.

The testing case at $\eta = 0$ reveals conventional counterpart wave propagation of u according to the d'Alembert solution with the velocity equal to a. As the values of η increases (that means that influence of the added mass increases), two differences in the wave dynamics are realized. First, the velocity of the counterpart waves gradually decreases. Second, an amplitude of the moving waves increases. Finally, a standing oscillating part appears in the area of the initial perturbation around x_0. Figure 3 shows the wave evolution at $\eta = 0.5$. For comparison, propagation of the wave at $\eta = 0$ with the velocity equal to a is shown by dashed line.

The computations show that the localized waves propagate with a permanent velocity keeping their shape, see Fig. 4a. The influence of the added mass is not only in a decrease in the velocity but also in an appearance of the oscillating standing part in the vicinity of the initial condition position, $x = x_0$. Such behavior depends on the parameter k of the initial conditions (12)–(13). Shown in Fig. 4 is the splitting on two opposite propagating waves for different values of the parameter k of the Gaussian distribution. As the case in Fig. 4a demonstrates equal amplitude of the waves moving in the opposite directions, an increase in k in Fig. 4b results in an appearance of the oscillations behind the moving waves. Nevertheless, the amplitude of the waves remains permanent. Further increase in k gives rise to appearance of the developing oscillating tail behind the traveling waves while oscillations in the area around x_0 disappear, see Fig. 4c. Let us note that the greater is value of the parameter k, the higher is the initial localization. This might be cause for the oscillation tails and the time decrease of the traveling wave amplitude, observed for the higher values of k—see Fig. 4c.

Use of the higher value of η for the last case from Fig. 4c results in a more complicated dynamics shown in Fig. 5. One can see in Fig. 5b that the moving wave has the amplitude higher than that at $\eta = 0$ similar to the case shown in Fig. 3b. However, as times goes on, the amplitude of the wave decreases and becomes lower than that of the case $\eta = 0$ shown in Fig. 5d. This is different from the case shown in Fig. 3d. Besides the
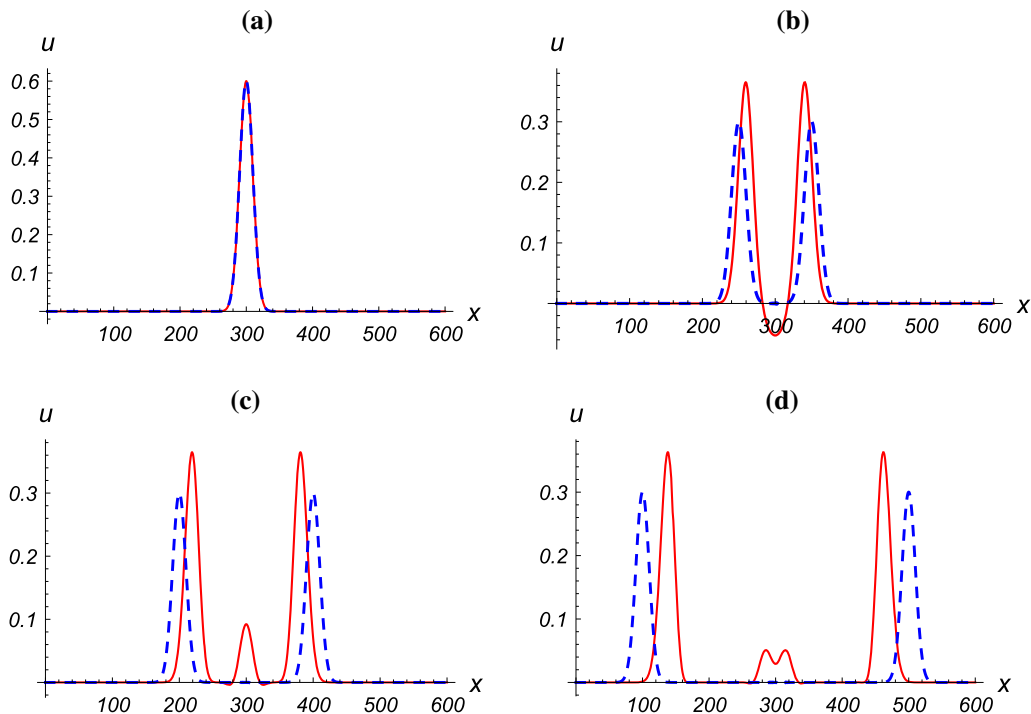
Fig. 3 Formation of two localized waves for $\eta = 0.5$ (red solid line) and $\eta = 0$ (blue dashed line): **a** $t = 0$, **b** $t = t_N/4$, **c** $t = t_N/2$, **d** $t = t_N$. Here $t_N = 400$ units of time (color figure online)
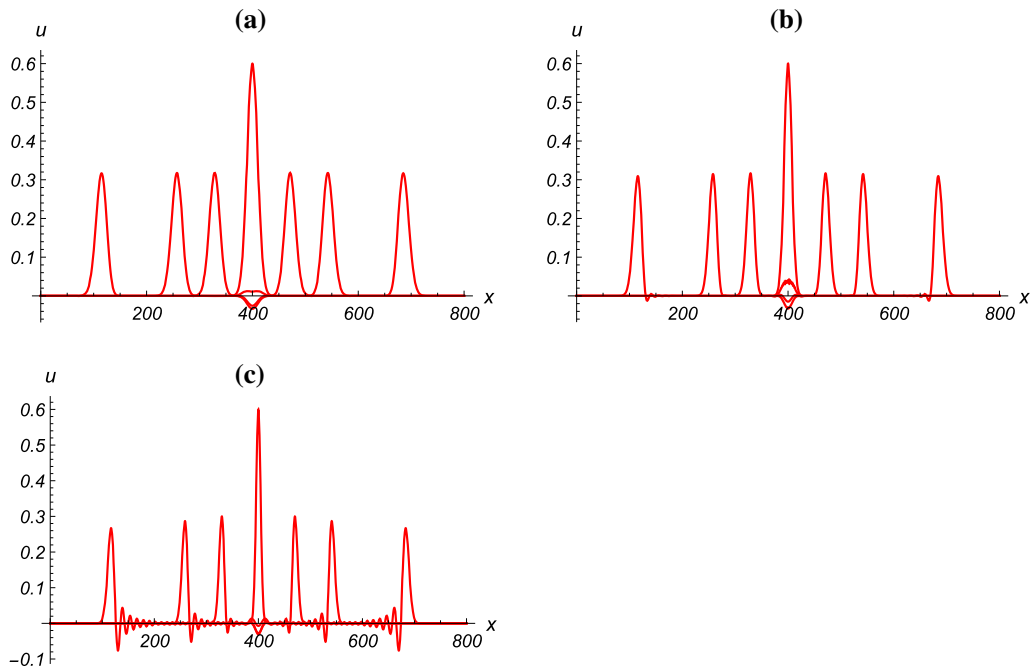
Fig. 4 Splitting into counterpart waves for different values of k: **a** $k = 0.005$, **b** $k = 0.01$, **c** $k = 0.027$. Each figure shows superposition of results calculated for the sequential moments of t, namely: 0, $t_N/4$, $t_N/2$, t_N. Here $t_N = 600$ units of time
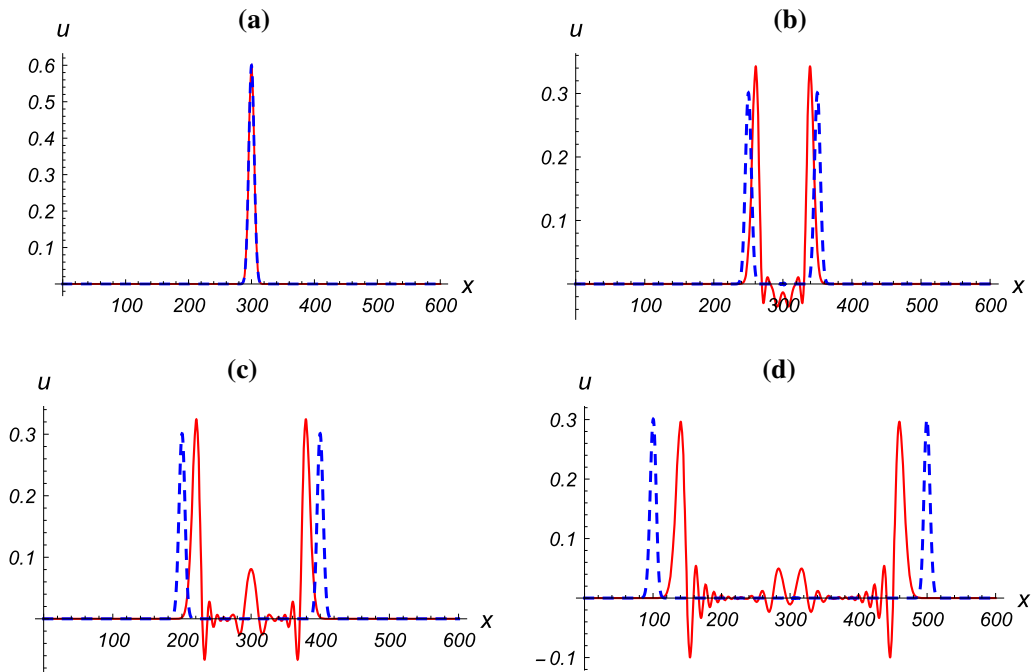
Fig. 5 Decrease in the amplitude of localized waves and development of oscillating tails at $\eta = 0.5$ (solid red line) and $\eta = 0$ (dashed blue line). In both cases $k = 0.027$. The frames correspond to **a** $t = 0$, **b** $t = t_N/4$, **c** $t = t_N/2$, **d** $t = t_N$. Here $t_N = 400$ units of time (color figure online)

developing tail similar to the case of Fig. 4c, the standing oscillatory part also exists like in the case shown in Fig. 3d.

Now we consider evolution of an initially localized perturbation in the form of the Gaussian distribution with nonzero conditions on the first temporal derivative, which are chosen in correspondence with Eq. (10):

$$u(x, 0) = F \exp\left(-k(x - x_0)^2\right), \qquad u_t(x, 0) = 2FkW(x - x_0) \exp\left(-k(x - x_0)^2\right), \tag{14}$$

$$v(x, 0) = G \exp\left(-k(x - x_0)^2\right), \qquad v_t(x, 0) = 2GkW(x - x_0) \exp\left(-k(x - x_0)^2\right). \tag{15}$$

We choose $k = 0.01$ and $\eta = 0.1$ for these simulations while the values of the remaining parameters are assumed to be the same as before. Figure 6 shows the evolution at two different initial velocities: $W = 0.1$ (dashed blue line) and

$W = a_1 \approx 0.44$ (solid red line). The second value of W is chosen to provide a unidirectional propagation similar to Eq. (11). Indeed, in the case $W = 0.1$ we have a permanent amplitude wave moving to the left with a higher amplitude than the wave moving to the right. At the same time, in the second case, the amplitude of the wave moving to the left increases, while the wave moving in the opposite direction disappears. Further increase in the value of W results in the negative amplitude wave propagation to the left. The wave fronts in both directions propagate with the same velocity equal to a_1, clearly demonstrating the long-wave limit. Meanwhile some of oscillations remain standing and they are almost the same for both considered values of the velocity. Also the well-pronounced oscillation tails appear behind the traveling waves.

Figure 7 shows the temporal evolution of the waves with the decreasing amplitude at the parameter of the initial condition $k = 0.027$ and different initial velocities. A decrease in the wave amplitude happens in both directions and both for positive and negative sign of the amplitude. Main part of the oscillations develop behind the traveling waves, only a small part remains standing around the point of the position of the initial perturbation.

Similar to Fig. 6, it is observed that if the initial velocity W is not equal to the long-wave acoustic limit a_1, then two localized traveling waves are generated, one moving forward, second—backward. The sign of the backward wave amplitude depends on the difference between W and a_1, similarly to that shown by Eq. (11). Thus, the initial conditions Eqs. (14), (15)), being designed for both masses according to Eq. (10), result in a unidirectional localized wave, when and only when the initial velocity W is exactly equal to the long-wave acoustic limit a_1.
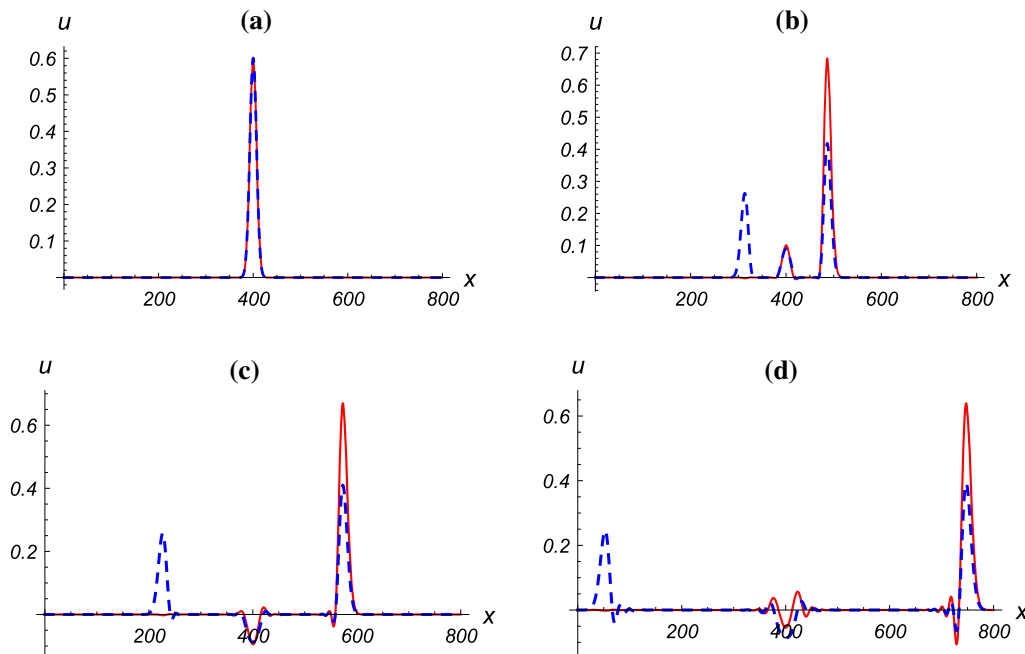
Fig. 6 Comparison of the wave dynamics for two different initial velocities W at $\eta = 0.1$, $k = 0.01$. Case $W = 0.1$ is shown by the blue dashed line, $W = a_1$—by the red solid line. The frames correspond to the sequential moments of time: **a** $t = 0$, **b** $t = t_N/4$, **c** $t = t_N/2$, **d** $t = t_N$. Here $t_N = 800$ units of time (color figure online)
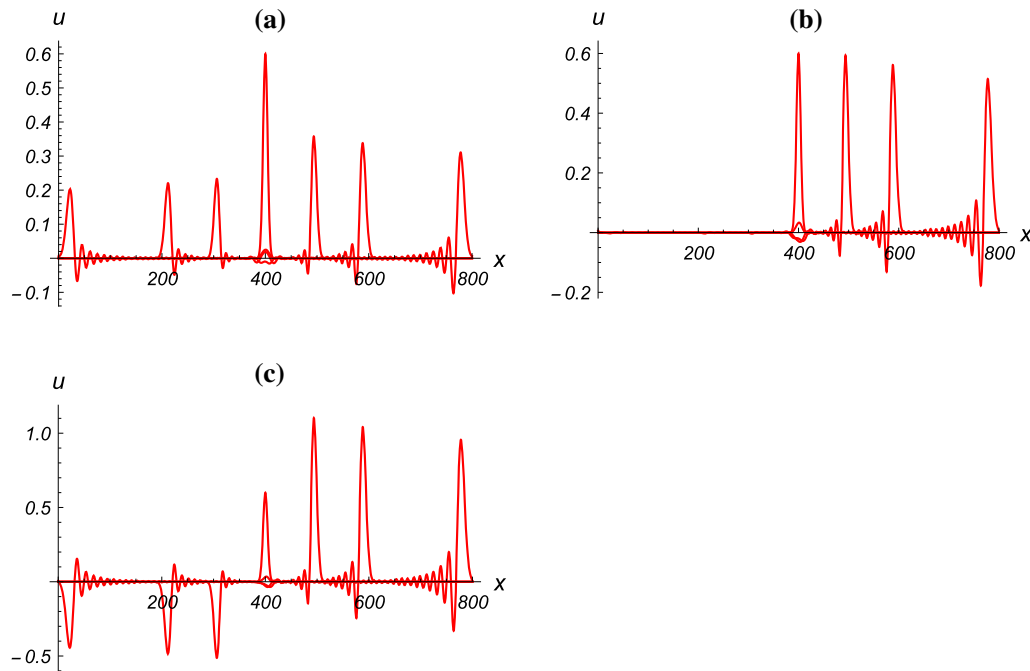
Fig. 7 Comparison of the wave dynamics for two different initial velocities W at $k = 0.027$, $\eta = 0.1$. **a** $W = 0.1$, **b** $W = a_1 \approx 0.44$, **c** $W = 1.3$. Each figure shows superposition of results calculated for the sequential moments of t, namely: 0, $t_N/4$, $t_N/2$, t_N. Here $t_N = 800$ units of time

4 Discussion and concluding remarks

We study propagation of the dispersive localized waves in a system governed by a long wavelength continuum limit of the discrete system with attached masses. Of special interest is to see how an analysis based on the harmonic wave solution could be used for explanation of the features of the numerical solution for localized waves.

Let us summarize the results of numerical simulations. Despite the dispersion in the considered system, the localization of the traveling waves can be kept for the distances, far greater than the width of the wave. Localized waves propagate with the velocity equal to $a_1 = a/\sqrt{1 + \eta}$ independently of the value and the sign of its amplitude. However, such scenario depends on the parameters of the initial pulse: Higher values of the parameter k (see Fig. 4) give rise to the scenario, which is more conventional for dispersive systems, when the amplitude of the traveling wave decreases with time, and the oscillating tail appears behind the wave. We also observe standing oscillations around the point related to the position of the initial perturbation. Band gap is not reached in the numerical simulations.

The observed features of the numerical solutions better relate to the analytical predictions done on the basis of the group velocity, rather than the phase velocity—see Table 1. Indeed, the long-wave limiting values of the group and the phase acoustic velocities are the same. The standing oscillations could be explained as an evidence of the wave corresponding to the optical group velocity, whose limiting long-wave value is zero, see Fig. 2. Finally, there is no band gap for the group velocity similar to the numerical results.

The band gap is described analytically on the basis of a single mode periodic solution. Numerically we study evolution of a localized wave. It is possible to represent the localized wave in the Fourier series or the integral; however, the modes in the series or in the integral will lie both inside and outside the ban gap. Probably, this is a reason why there is no evidence of the band gap in the numerical evolution of the localized waves.

We would like to demonstrate an absence of a bang gap for a localized input evolution, and we use only the Gaussian initial distribution. It might be of interest to consider other localized shapes, e.g., the δ- shape in a closer relation to the limit $p \to \infty$. Also the future work concerns an analysis of the energy transfer for the localized traveling waves that have been considered above in a harmonic approximation. Important question is connected with the energy transfer between the degrees of freedom [30] and with existence of the

additional conservation laws, such as the global energy flux conservation [27]. Further investigations can be associated with an inclusion of nonlinear terms in the original model to obtain the soliton-like localized waves with permanent amplitude, arising as a balance between nonlinearity and dispersion.

References

1. Born, M., Huang, K.: Dynamical Theory of Crystal Lattices. Clarendon Press, Oxford (1954)
2. Askar, A.: Lattice Dynamical Foundations of Continuum Theories. World Scientific, Singapore (1985)
3. Ostoja-Starzewski, M.: Lattice models in micromechanics. Appl. Mech. Rev. **55**, 35–60 (2002)
4. Alibert, J.-J., Seppecher, P., Dell'Isola, F.: Truss modular beams with deformation energy depending on higher displacement gradients. Math. Mech. Solids **8**, 51–73 (2003)
5. Askes, H., Metrikine, A.V.: Higher-order continua derived from discrete media: continualisation aspects and boundary conditions. Int. J. Solids Struct. **42**, 187–202 (2005)
6. Krivtsov. A.M.: Deformation and fracture of solids with microstructure. Fizmatlit, Moscow(2007) (**in Russian**)
7. Andrianov, I.V., Awrejcewicz, J., Weichert, D.: Improved continuous models for discrete media. Math. Probl. Eng. (Open Access) 986242 (2010)
8. Michelitsch, T.M., Collet, B., Wang, X.: Nonlocal constitutive laws generated by matrix functions: lattice dynamics models and their continuum limits. Int. J. Eng. Sci. **80**, 106–123 (2014)
9. Lepri, S. (ed.): Thermal Transport in Low Dimensions: From Statistical Physics to Nanoscale Heat Transfer. Lecture Notes in Physics **921**. Springer International Publishing, Switzerland (2016)
10. Krivtsov, A.M.: The ballistic heat equation for a one-dimensional harmonic crystal. In: Altenbach, H. et al. (eds.), Dynamical Processes in Generalized Continua and Structures, Advanced Structured Materials **103**, 345–358, Springer Nature Switzerland AG (2019)
11. Kuzkin, V.A.: Unsteady ballistic heat transport in harmonic crystals with polyatomic unit cell. Continuum Mech. Thermodyn. **31**, 1573–1599 (2019)
12. Panchenko, AYu., Kuzkin, V.A., Berinskii, I.E.: Unsteady ballistic heat transport in two-dimensional harmonic graphene lattice. J. Phys. Cond. Matter. **34**, 165402 (2022)
13. Cveticanin, L., Cveticanin,D.: Acoustic Metamaterials: Theory and Application. In: Herisanu, N., Marinca, V. (eds.), Acoustics and Vibration of Mechanical Structures-AVMS-2017. Springer Proceedings in Physics 198 (2018)
14. Huang, H.H., Sun, C.T., Huang, G.L.: On the negative effective mass density in acoustic metamaterials. Int. J. Eng. Sci. **47**, 610–617 (2009)
15. Ma, G., Sheng, P.: Acoustic metamaterials: from local resonances to broad horizons. Sci. Adv. **2**(2), 1–16 (2016)
16. dell'Isola, F., et al.: Pantographic metamaterials: an example of mathematically driven design and of its technological challenges. Continuum Mech. Thermodyn. **31**, 851–884 (2019)
17. Eremeyev, V.A., Turco, E.: Enriched buckling for beam-lattice metamaterials. Mech. Res. Commun. **103**, 103458 (2020)
18. Nejadsadeghi, N., Placidi, L., Romeo, V., Misra, A.: Frequency band gaps in dielectric granular metamaterials modulated by electric field. Mech. Res. Commun. **95**, 96–103 (2019)
19. Madeo, A., et al.: First evidence of non-locality in real band-gap metamaterials: determining parameters in the relaxed micromorphic model. Proc. R. Soc. Lond. Ser. A, **47**(2), 20160169 (2016)
20. Kaviany, M.: Heat Transfer Physics, 2nd edn. Cambridge University Press, New York (2014)
21. Guo, Y., Wang, M.: Phonon hydrodynamics and its applications in nanoscale heat transport. Phys. Rep. **595**, 1–44 (2015)
22. Anufriev, R., Ramiere, A., Maire, J., Nomura, M.: Heat guiding and focusing using ballistic phonon transport in phononic nanostructures. Nat. Commun. **8**, 15505 (2017)
23. Saito, R., Mizuno, M., Dresselhaus, M.S.: Ballistic and diffusive thermal conductivity of graphene. Phys. Rev. Appl. **9**(2), 024017 (2018)
24. Zhang, Z., et al.: Size-dependent phononic thermal transport in low-dimensional nanomaterials. Phys. Rep. **860**, 1–26 (2020)
25. Kuzkin, V.A., Krivtsov, A.M.: Unsteady ballistic heat transport: linking lattice dynamics and kinetic theory. Acta Mech. **32**(5), 1983–1996 (2021)
26. Kunin, I.A. : Elastic Media with Microstructure. I. One-dimensional models. Springer Series in Solid-State Sciences, vol. 1, 2. Springer-Verlag, Berlin, Heidelberg (1982)
27. Krivtsov, A.M.: Dynamics of matter and energy. Z. Angew. Math. Mech. e202100496 (2022)
28. El Sherbiny, M., Placidi, L.: Discrete and continuous aspects of some metamaterial elastic structures with band gaps. Arch. Appl. Mech. **18**, 1725–1742 (2018)
29. Placidi, L., Galal el Sherbiny,V., Baragatti, P.: Experimental investigation for the existence of frequency band gap in a microstructure model. Mathematics and Mechanics of Complex Systems, **9**, 413–422 (2021)
30. Kuzkin, V.A.: Thermal equilibration in infinite harmonic crystals. Continuum Mech. Thermodyn. **31**, 1401–1423 (2019)